

A Feature Preserved Mesh Subdivision Framework for Biomedical Mesh

Jing Yang[†], Yongyi Gong[†], Hefeng Wu[†], and Qi Li[‡]

[†]School of Information Science and Technology, Guangdong University of Foreign Studies, China

[‡]Department of Computer Science, Western Kentucky University, Bowling Green, KY, USA

jingyang.carl.china@gmail.com, gongyongyi@gdufs.edu.cn, wuhfeng@gmail.com, qi.li@wku.edu

Abstract—As biomedical data in 3D space collected increasingly, there is a pressing need for efficient and accurate applications in the field of bioinformation analysis. For biomedical purpose, mesh subdivision techniques are commonly used to generate adaptive multi-resolution meshes for fast or accurate algorithms. However, current smoothing methods for each subdivision algorithm will moderate edge and vertex features from the original mesh. In this paper, we propose a feature preserved mesh subdivision framework, which generates a visually sensitive and a more precise result compared with commonly used subdivision methods, to preserve edge and vertex geometrical features of biomedical data.

Index Terms—mesh subdivision, keypoints, feature preserved, biomedical mesh

I. INTRODUCTION

In recent years, 3D computer graphical technology works diffusely as biomedical assistants, including utilizations of three dimensional CT (3D CT) reconstructions [1]–[4], presentations of skeletons and tissues [5], comparisons of genome [6]–[9], etc., due to its visual obviousness. The technique is widely used for presenting facial bones and their connections, confirmation of borderline or size of diseased tissues and their relation to the adjacent tissues. With the aid of bio-images and bio-models, diagnosis and operations on clinical medicine achieves a much higher precision. Moreover, substantial effort has been made around world to determine spatial expression patterns of genes in mammalian genome using experimental techniques such as *in situ* hybridization (ISH) [10]. Performing ISH on multiple subjects yields expression images of various genes over the common anatomical structure and comparing these images reveals the spatial relations between genes, which are often key to understanding their functional relations [11], [12].

The pros of using computer graphics including 3D spatial and triangular meshes [13]–[15] to expose the nicety of bioinformation has created an ever-titanic amount of spatial data (in the form of 2D medical images and 3D bio-models) which requires efficient and accurate processing and analysis consequently. The anatomical differentiations among these biomedical models aggravate the computational challenges involved in visual and medical comparison among data collected from different modes [16].

Restrained by the calculation performance of physical devices, medical detailed expression and accuracy of biomedical

data is unfavorably circumstanced. Solutions emerge as medical processing requires, one of which is using meshes without redundant vertices and faces. The contradiction of biomedical precision and data optimization will become serious as models shrink. Hence, feature-based mesh subdivision present state-of-the-art results [16].

Using feature-based subdivision to suitably amplify medical precision and organize spatial data into multi-resolution versions, visual comparison and diagnosis will have a higher performance [16]. Meanwhile, the multi-resolution structure of a subdivision mesh further gives rise to fast algorithms for processing and accurate comparison for tiny bio-divergence.

Commonly used mesh subdivision methods including Butterfly method [17], Loop subdivision [18], and Catmull-Clark subdivision [19], whose experimental results are illustrated in Fig. 1. Moreover, Xie et al. [20] provided a solid-shell element based triangular subdivision to avoid interpenetration. Liu [21] introduced a dense reconstruction algorithm for mesh subdivision. Amresh et al. [22] developed a subdivision scheme derived from Loop scheme and using watershed segmentation. Rose et al. [23] proposed an adaptive process that stores the next splitting vertex and temporary triangle based on Modified Butterfly scheme. Kobbelt [24] developed refinement for both his Kobbelt scheme and newly introduced $\sqrt{3}$ subdivision. Seeger and Kai [25] introduced a subdivision scheme based on Butterfly Scheme using quark. In their method, subdivision is controlled by the faces of the original mesh and mesh features that are not suitably preserved.

In this paper, we propose a feature preserved mesh subdivision framework to maintain geometrical features, including edges and imbalanced vertices, of original biomedical meshes while giving out a more adaptive mesh derivative. Our contributions include: a) imbalanced keypoint detection for point feature preservation, b) edge feature preserved mesh subdivision for edge feature preservation, and c) model-dependent wavelike noise elimination for result optimization. Subdivision results will be compared after the same number of iterations and results show the promise of our method on feature maintained mesh subdivisions.

II. COUPLING MODULES OF SUBDIVISION FRAMEWORK: FUNDAMENTAL SUBALGORITHMS

In this section, we will give an overview of algorithm modules within the proposed framework where Imbalanced

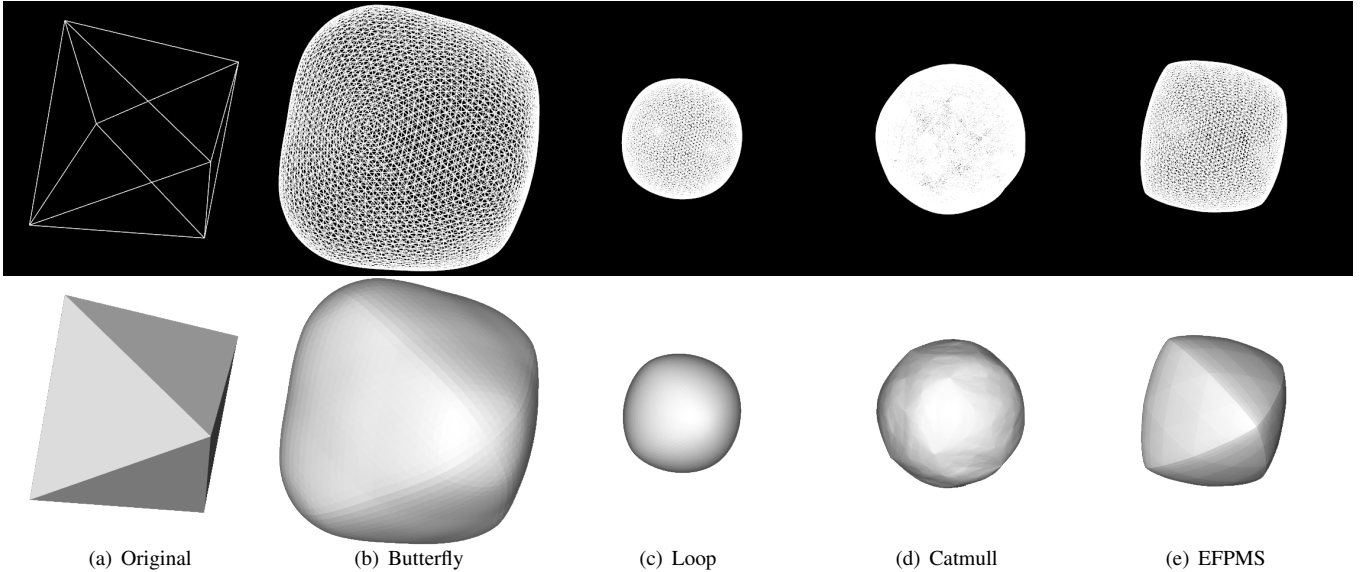


Fig. 1: Demonstration of different subdivision methods. a) Original Mesh. b) Butterfly Subdivision. c) Loop Subdivision. d) Catmull Subdivision. e) Edge Feature Preserved Mesh Subdivision (implementation of our framework's core module). All subdivision algorithms have been applied five iterations on original mesh.

Keypoint Detection focuses on vertex features while Edge Feature Preserved Mesh Subdivision (EFPMS) underscores edge features. A brief introduction on imbalanced-vertex based feature detection will first be presented and then our algorithm kernel, EFPMS, are provided, while a corresponding optimization solution is proposed afterward to eliminate model-dependent wavelike noise generated from that. Moreover, the kernel module follows subdivision scheme composed of linear triangular face subdivision and vertex smoothing.

A. Imbalanced Keypoint Detection

We first propose a geometric feature-based vertex operator, which is a three-dimensional implementation of keypoints detection, to pick up imbalanced keypoints. We extend Li's previous work [26] on imbalanced keypoints detection to triangular meshes.

The basic idea of vertex operator is using projections to transform 3D geometric features to two-dimensional space. Let $M(V, F, N_F)$ be a triangular mesh where V is the set of vertices, F is the set of faces, and N_F represents the set of face normals. Suppose a projection P_T will project any vector onto the plane T , 3D geometric mesh features will be transformed to two dimensions when T is the tangent plane of the given mesh vertex in vertex set V . Face normals N_F will then be transformed into its projected vector set N_F' . Finally, we settle all normalized vectors in N_F' to a polar coordinate system and calculate the set of cross angles between each vector side by side, denote as A_F .

Imbalanced point selection in 2D images aims to minimize the occurrences of edge points [26] as illustrated in Fig. 2. Denote I a grayscale image, p a local point, $\theta_i = \frac{(i-1)2\pi}{N}$, and $l_i = (\cos \theta_i, \sin \theta_i)$ for $i = 1, 2, \dots, N$. Denote $\frac{\partial I}{\partial l_i}(p)$

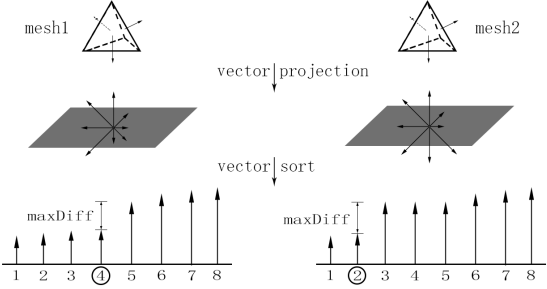


Fig. 2: Illustration of imbalance selection. After projecting face normals around vertex on its tangent plane, projected normals (suppose 8 directions) are sorted in terms of their magnitudes. Left: balanced edge point, where index of maximum difference is 4. Right: imbalanced edge point, where that is 2.

a directional derivative of p along l_i direction. We cluster $\{\frac{\partial I}{\partial l_i}(p)\}_{i=1}^N$ into two classes in terms of their magnitudes $|\frac{\partial I}{\partial l_i}(p)|$. If two clusters have the same size, the image point p is balanced.

The sorting method proposed in Li's method is to classify $\{\frac{\partial I}{\partial l_i}(p)\}_{i=1}^N$, which can be generalized to extract 3D imbalanced vertices with proposed operator. Let $maxDiff$ be the max difference and D be the index of maximum difference:

$$maxDiff = \max_j(\alpha_{j+1} - \alpha_j) \quad (1)$$

$$D = \arg \min_j(\alpha_{j+1} - \alpha_j) \quad (2)$$

where α represents value in A_F , and $1 \leq j \leq N - 1$. Given a threshold on homogeneity ε , the imbalanced vertex can be defined under the condition that $\maxDiff < \varepsilon$:

$$IMB(v_i) = \begin{cases} 1 & D_i < \frac{N}{2} \\ 0 & \text{else} \end{cases} \quad (3)$$

One of the implementation results is presented in Fig. 3 where imbalanced keypoints delineate vertex features.

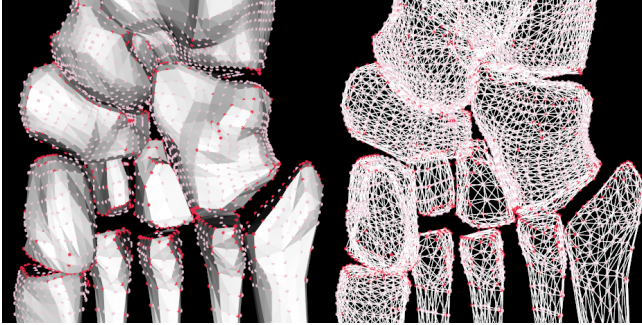


Fig. 3: Imbalanced keypoints on footbone mesh with white points representing normal points and red for imbalanced points. Left: model view. Right: mesh view.

B. Edge Feature Preserved Mesh Subdivision

Loops method [18] can be expressed as linear subdivision and an averaging scheme to approximate a spherical surface, which will efface edge and vertex features. The phenomenon is common when applying Catmull method and Butterfly method. When the mesh is rigid, these iterations will fail to preserve the original geometrical features as illustrated in Fig. 1. To moderate the feature friction after subdivision and highlight original edge and vertex features, we provide an Edge Feature Preserved Mesh Subdivision (EFPMS) method to generate feature adaptive results, where the pseudocode is arranged in Algorithm 1.

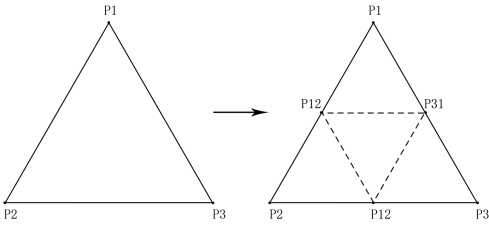


Fig. 4: Linear one to four subdivision for triangulants.

Our proposed method implements linear one to four triangular mesh subdivisions to increase the details in a mesh as illustrated in Fig. 4, and then smooths it to accomplish surface approximation after subdivision while actualizing shape retention.

Denote the original mesh as M_i , and the edge point generator G_{EFPMS} is depicted in Fig. 7. To perform linear triangular subdivision, we insert points created by generator G_{EFPMS}

on the edge of each triangle to the hash map $H_n(v_i, h_i)$ for storing vertices v_i and their handles h_i as corresponding hash keys. For each vertex on mesh $\{v_1, v_2, \dots, v_n\}$, we check whether the generated middle edge point v_k is already in the map. If so, we get its handle h_k for the on-coming face generation, and otherwise insert the point v_k into the mesh and create its handle h_k while updating vertices hash map $H_{n+1}(v_i, h_i)$. Finally, the new triangular surfaces are formed using vertex handles geometrically anticlockwise, and older redundant faces are eliminated simultaneously. Each triangle will then be split into four sub-triangles and original mesh M_i is subdivided to M_{i+1} .

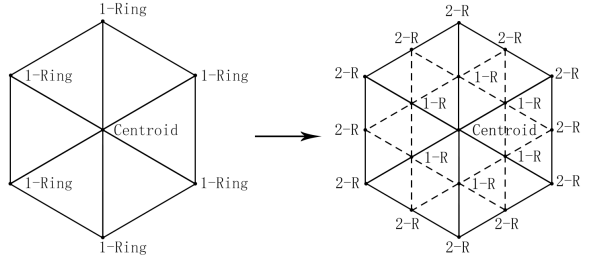


Fig. 5: One-ring vertices derivative.

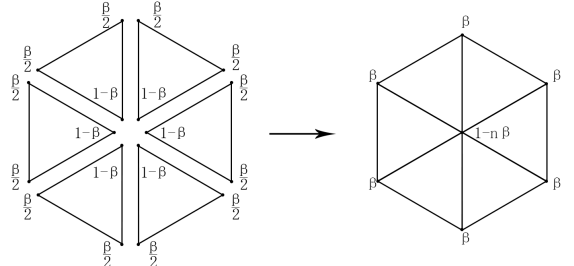


Fig. 6: One-ring neighbor weighted centroid method.

Smoothing for triangular meshes will be applied to not only the previous vertices on M_i but also all vertices on the generated mesh M_{i+1} whose two-ring vertex set is derived from one-ring vertices of previous mesh M_i as illustrated in Fig. 5. For each vertex on M_{i+1} , we use a one-ring neighbor weighted centroid method for averaging as shown in Fig. 6. The weight of each neighbor β is decided by the number of one-ring neighbors n :

$$\beta = \frac{5}{8} - \left(\frac{3}{8} + \frac{1}{4} \cos \frac{2\pi}{n} \right)^2 \quad (4)$$

C. Model-dependent Wavelike Noise Elimination

By using EFPMS, an edge and vertex aware result is generated. But the method will generate model-dependent wavelike noise on the mesh, as illustrated in Fig. 8.

We propose Model-dependent Wavelike Noise Elimination, a combination of EFPMS and Smoothness-focused Mesh Subdivision (SMS), to eliminate noise. The subdivision scheme consists of several iterations of EFPMS and an iteration of

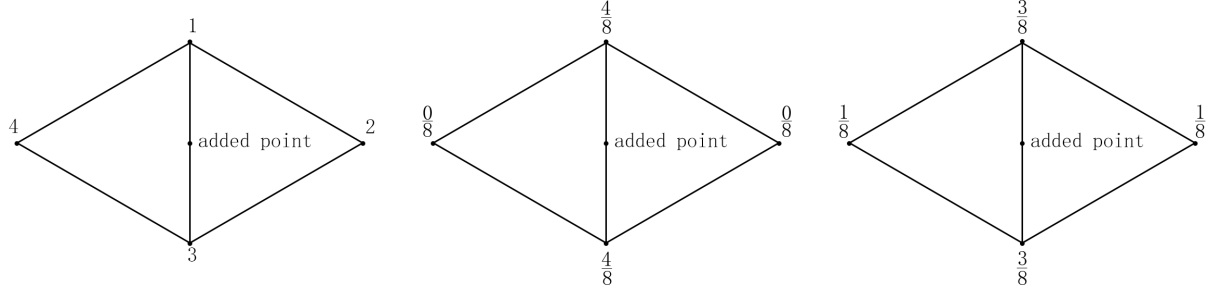


Fig. 7: Unit of edge point generator (left). Feature Preserved Mesh Subdivision edge point generator (middle). Smoothness-focused Mesh Subdivision edge point generator (right). Weight of vertices in each generator are tagged aside its position.

Algorithm 1 Edge Feature Preserved Mesh Subdivision

Input : Original Mesh M_i
Output : Subdivided Mesh M_{i+1}

for each triangular face f_i **in** M_i **do**
 get 3 edge point on edges of f_i with G_{FPMS} ;
 generate 4 subsurfaces anticlockwise;
end for
 {NOTE: M_i is now subdivided into M_{i+1} }

for each vertex v_i **in** M_{i+1} **do**
 $N(v_i)$ = 1-ring neighbors of v_i on current mesh M_{i+1} ;
 v_i = 1-ring Neighbor Weighted Centroid method on v_i ;
end for
 {NOTE: M_{i+1} is now smoothed}

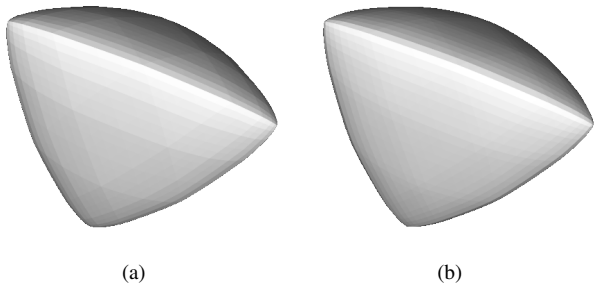


Fig. 8: a) Model-dependent wavelike noise. b) Removing wavelike noise by Smoothness-focused Mesh Subdivision. All subdivision algorithms have been applied five iterations on original meshes.

SMS at the end of the algorithm. The implementation of SMS resembles the EFPMS, except the generation of edge points and smoothing operator.

Unlike edge points generator G_{EFPMS} in feature preserved subdivision, edge points in the last iteration of noise elimination algorithm are generated based on weighted neighbors illustrated in Fig. 7, where directly connected vertices take up a greater weight, namely $3/8$ each, and indirect weight is slightly less, namely $1/8$ each.

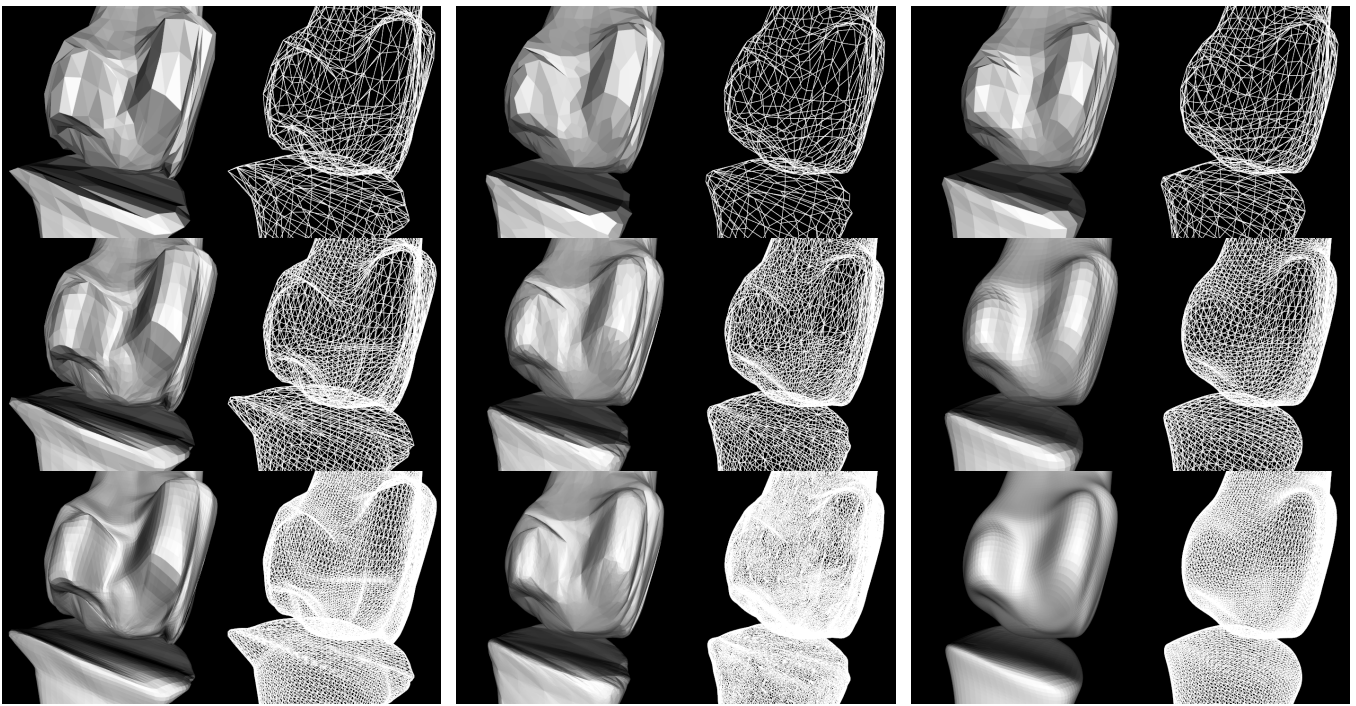
Neighbor vertices in the smoothing method depend on previous one-ring vertices on M_i , but not newly generated vertices on M_{i+1} , which is different from the implementation of EFPMS. The weight of each neighbor follows the same principle introduced in EFPMS.

III. FEATURE PRESERVED MESH SUBDIVISION FRAMEWORK

In this section, we propose a Feature Preserved Mesh Subdivision Framework (FPMS), which contains edge point generation and smooth operator, to balance the emphasis of original features and smoothing extent. The big picture of our framework is using detected points to guide subdivision procedures. Based on imbalanced keypoint detection, all the vertices are classified into two categories, and keypoints are distributed mainly at the boundaries and detailed parts, which should be kept after subdivision but slightly adjusted with neighbors. The proposed FPMS framework is depicted in Algorithm 2.

The unit of edge point generation in our provided method is a couple of triangles back to back as illustrated in Fig. 7. Denote edge point generators in Edge Feature Preserved Mesh Subdivision and Smoothness-based Mesh Subdivision as $G_{EFPMS}(N)$ and $G_{SMS}(N)$ respectively, where N is the set of neighbor points.

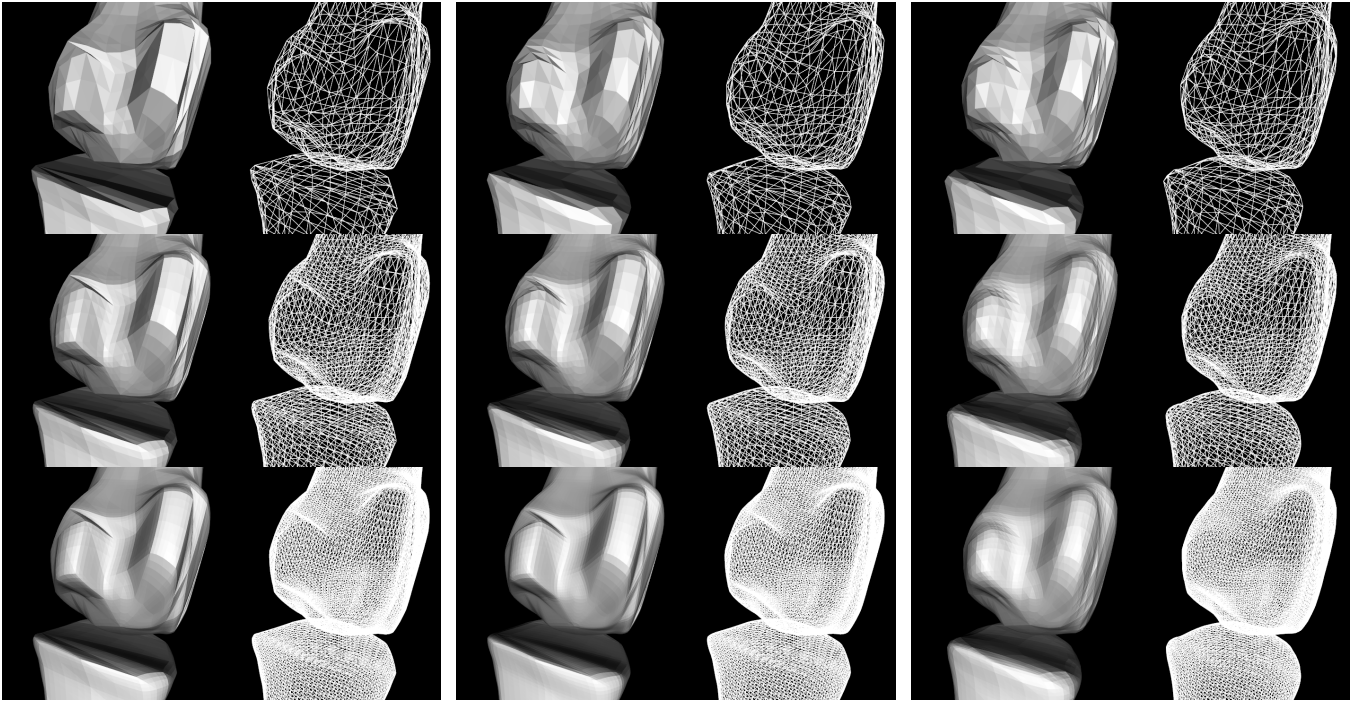
The balance can be guided by the amount of imbalanced keypoints in an isolated generation unit and implemented by a weighted combination of $G_{EFPMS}(N)$ and $G_{SMS}(N)$. For a precise and accurate calculation, the weight of two generators should be geometrically related and symmetric. The weight of $G_{EFPMS}(N)$ and $G_{SMS}(N)$ will be defined as $W_{G_{EFPMS}}$



(a) Butterfly

(b) Catmull

(c) Loop



(d) EFPMS

(e) SMS

(f) FPMS

Fig. 9: Subdivision Comparison on phalangeals with iteration increasing by rows. a) Butterfly Method. b) Catmull Method. c) Loop Method. d) Edge Feature Preserved Mesh Subdivision. e) Smoothness-focused Mesh Subdivision. f) Feature Preserved Mesh Subdivision.

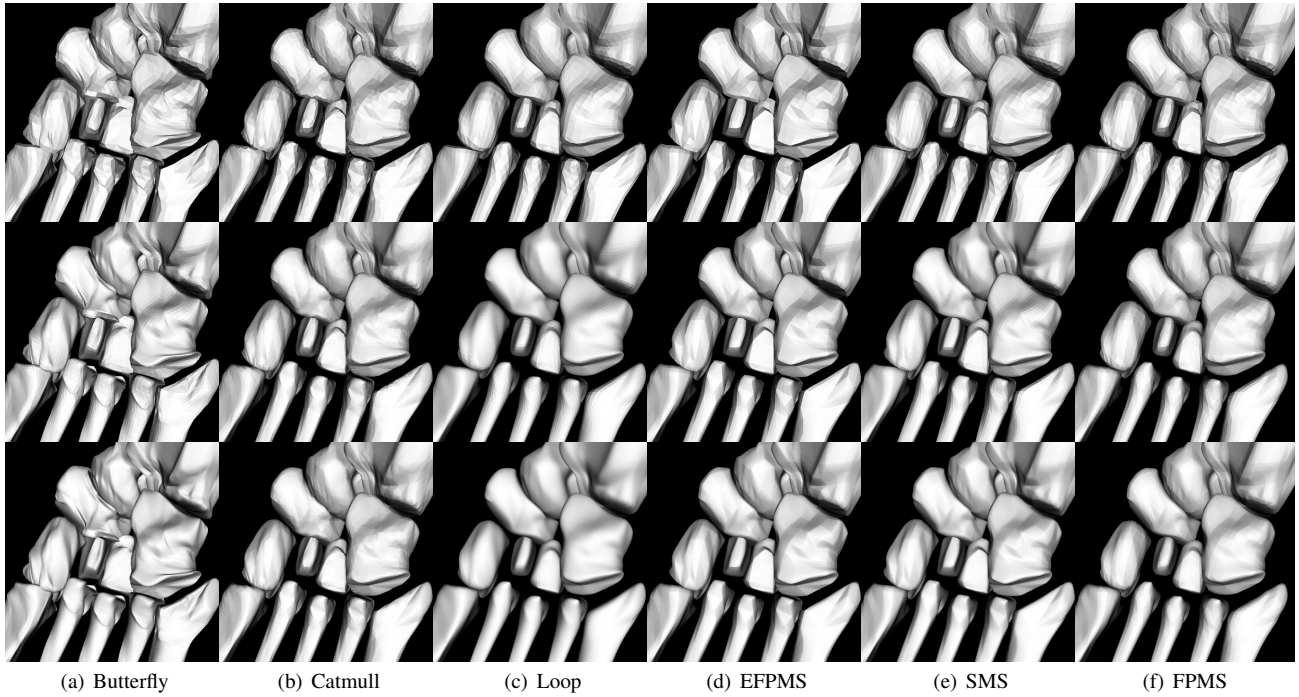


Fig. 10: Subdivision Comparison on human footbone with iteration increasing by rows. a) Butterfly Method. b) Catmull Method. c) Loop Method. d) Edge Feature Preserved Mesh Subdivision. e) Smoothness-focused Mesh Subdivision. f) Feature Preserved Mesh Subdivision.

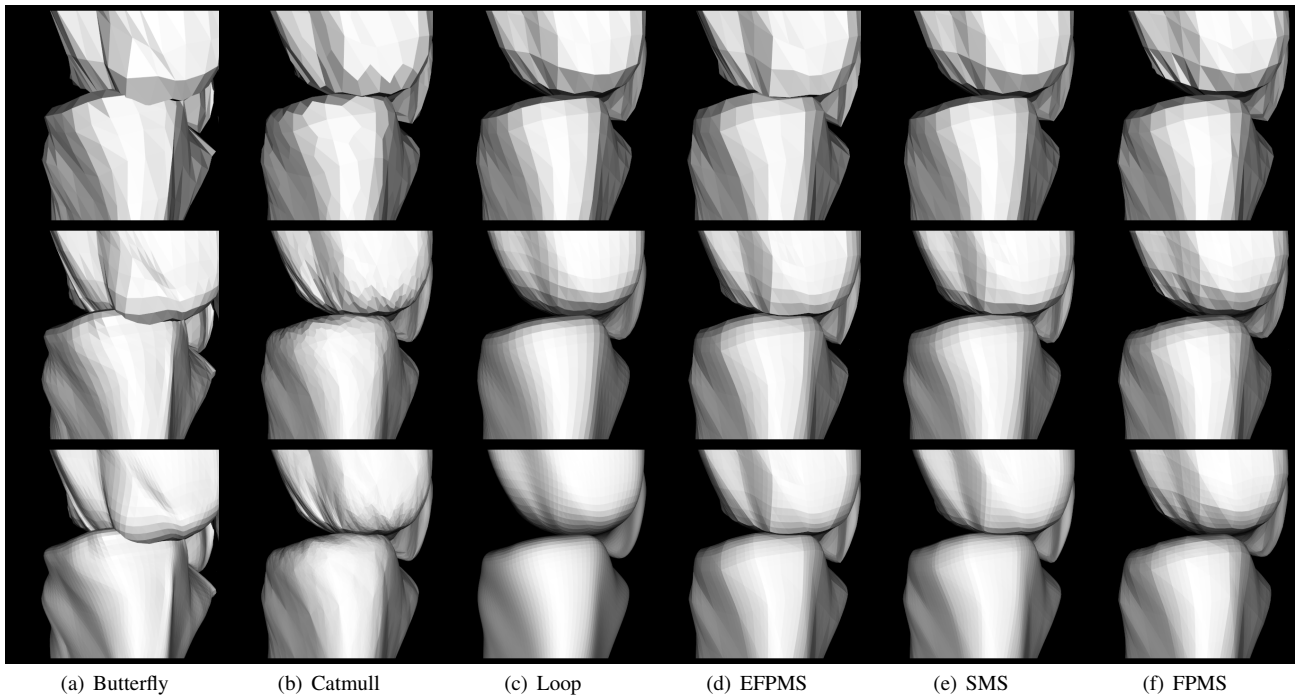


Fig. 11: Subdivision Comparison on metatarsal bones and entocuneiforms with iteration increasing by rows. a) Butterfly Method. b) Catmull Method. c) Loop Method. d) Edge Feature Preserved Mesh Subdivision. e) Smoothness-focused Mesh Subdivision. f) Feature Preserved Mesh Subdivision.

and $W_{G_{SMS}}$, which depend on the number of keypoints in a generation unit, and obey the following principles.

$$W_{G_{EFPMS}} = \sum_{i=1}^{|N|} Key(N_i) \quad (5)$$

$$W_{G_{SMS}} = |N| - \sum_{i=1}^{|N|} Key(N_i) \quad (6)$$

$$Key(N_i) = \begin{cases} 1 & N_i \text{ is a keypoint} \\ 0 & \text{else} \end{cases} \quad (7)$$

A combination of two edge point generator $G(N)$ will be defined as:

$$G(N) = W_{G_{EFPMS}} G_{EFPMS}(N) + W_{G_{SMS}} G_{SMS}(N) \quad (8)$$

Smooth operator will also be guided by keypoints, which extends the previous smoothing scheme. Neighbor vertices for smooth operator will be different, which depend on whether the centroid vertex is a keypoint or not. If so, neighbor vertices should be older one-ring vertices on M_i , and otherwise, one-ring vertices on M_{i+1} .

Algorithm 2 Feature Preserved Mesh Subdivision

Input : Original Mesh M_i
Output : Subdivided Mesh M_{i+1}

imbalanced keypoint detection on M_i ;
 {NOTE: vertices have been classified into two class}

```

for each triangular face  $f_i$  in  $M_i$  do
  get edge point  $e_{EFPMS}$  on edges of  $f_i$  with  $G_{EFPMS}$ ;
  get edge point  $e_{SMS}$  on edges of  $f_i$  with  $G_{SMS}$ ;
  average position of edge points by  $G(N)$ ;
  generate 4 sub-faces anticlockwise;
end for
{NOTE:  $M_i$  is now subdivided into  $M_{i+1}$ }

for each vertex  $v_i$  in  $M_{i+1}$  do
  if  $v_i$  is a keypoint then
     $N(v_i) = 1\text{-ring neighbors of } v_i \text{ on } M_i$ ;
     $v_i = 1\text{-ring Neighbor Weighted Centroid on } v_i$ ;
  else
     $N(v_i) = 1\text{-ring neighbors of } v_i \text{ on } M_{i+1}$ ;
     $v_i = 1\text{-ring Neighbor Weighted Centroid on } v_i$ ;
  end if
end for
{NOTE:  $M_{i+1}$  is now smoothed}
  
```

IV. EXPERIMENTS

We test different subdivision methods on several biomedical data, including phalanx, cuneiform bone, central anlrlle bone, cuboid bone, etc.

As the iteration number of subdivision methods increases, the performance of different algorithms becomes easier to differentiate, as illustrated in Fig. 9. Except Catmull method, all the subdivision methods implement one to four triangular subdivision, which means each mesh in a row has the same number of vertices and faces except the mesh generated by Catmull subdivision. The number of vertices and triangular faces in each iteration follows the below principles when applying one to four mesh subdivision schemes, where $V(\cdot)$ and $F(\cdot)$ represent total amount of vertices and faces on a mesh, respectively.

$$V(M_{i+1}) = V(M_i) + \frac{3}{2}F(M_i) \quad (9)$$

$$F(M_{i+1}) = 4F(M_i) \quad (10)$$

Obviously, the subdivision result of Loop method has a better sphere-like appearance, while EFPMS provides a better property of edge feature preservation. Butterfly subdivision leads the resulted mesh to a more boundary malleable shape, while Catmull presents more vertex details. Model-dependent Wavelike Noise Elimination accomplishes an edge feature preservation and smooth result, but compared with FPMS, the latter provides a better result on both edge and vertex features.

Fig. 10 and Fig. 11 exhibit more experimental comparisons on different meshes of biomedical utilizations. As illustrated in the figures, our proposed framework accomplishes a better result.

V. CONCLUSION

In this paper, we have presented a novel feature preserved mesh subdivision framework for processing biomedical mesh. The proposed Edge Feature Preserved Mesh Subdivision method works well on edge features but it will generate troublesome model-dependent noise waves. By using the idea in Smoothness-focused Mesh Subdivision, noise wave problems can be solved and it will generate a smoother result. By using imbalanced keypoints as guidance and incorporating EFPMS and SMS, our feature sensitive subdivision framework generates a better feature preserved result on both vertices and edges. The experimental results demonstrate that our method can provide more favorable results when compared with existing subdivision methods.

ACKNOWLEDGMENT

This work was supported by the National Natural Science Foundation of China (61370160, 61402120), the Natural Science Foundation of Guangdong Province (2015A030313578, 2014A030310348), and the Science and Technology Planning Project of Guangdong Province (2015B010106005).

The corresponding author is Yongyi Gong.

REFERENCES

- [1] Y. K. Choi and J. Cong, "Acceleration of EM-based 3D CT reconstruction using FPGA," *IEEE Transactions on Biomedical Circuits and Systems*, vol. 10, no. 3, pp. 754–767, 2016.
- [2] D. Koopman, J. Dalen, H. Arkies, A. B. Francken, J. Bart, S. Knollema, C. Slump, and P. Jager, "A small voxel FDG-PET/CT reconstruction improves the visual evaluation of axillary lymph nodes in patients with breast cancer," *Journal of Nuclear Medicine*, vol. 57, no. supplement 2, pp. 1502–1502, 2016.
- [3] P. Muthusami, N. Shkumat, V. Rea, A. H. Chiu, and M. Shroff, "CT reconstruction and MRI fusion of 3D rotational angiography in the evaluation of pediatric cerebrovascular lesions," *Neuroradiology*, vol. 59, no. 7, pp. 1–9, 2017.
- [4] M. T. Mccann, M. Nilchian, M. Stampanoni, and M. Unser, "Fast 3d reconstruction method for differential phase contrast X-ray CT," *Optics Express*, vol. 24, no. 13, pp. 14 564–14 581, 2016.
- [5] X. Tao, J. Yuan, and X. Yin, "Application of 3D CT reconstruction in maxillofacial surgery," *Acta Universitatis Medicinae Tangji*, 1999.
- [6] E. S. Lein, M. J. Hawrylycz, N. Ao, M. Ayres, A. Bensinger, A. Bernard, A. F. Boe, M. S. Boguski, K. S. Brockway, and E. J. Byrnes, "Genome-wide atlas of gene expression in the adult mouse brain," *Nature*, vol. 445, no. 7124, pp. 168–76, 2007.
- [7] B. Bonev and G. Cavalli, "Organization and function of the 3D genome," *Nature Reviews Genetics*, vol. 17, no. 11, pp. 661–678, 2016.
- [8] H. Tjong, W. Li, R. Kalhor, C. Dai, S. Hao, K. Gong, Y. Zhou, H. Li, X. J. Zhou, and G. M. Le, "Population-based 3D genome structure analysis reveals driving forces in spatial genome organization," *Proceedings of the National Academy of Sciences of the United States of America*, vol. 113, no. 12, pp. E1663–72, 2016.
- [9] J. Caspermeyer, "Principles of 3D genome folding and gene expression studied across species," *Molecular Biology and Evolution*, vol. 34, no. 6, pp. 1548–1548, 2017.
- [10] J. P. Carson, C. Thaller, and G. Eichele, "A transcriptome atlas of the mouse brain at cellular resolution," *Current Opinion in Neurobiology*, vol. 12, no. 5, pp. 562–565, 2002.
- [11] T. Ju, J. Warren, G. Eichele, C. Thaller, W. Chiu, and J. Carson, "A geometric database for gene expression data," in *Symposium on Geometry Processing*, 2003, pp. 166–176.
- [12] S. Schaefer, J. Hakenberg, and J. Warren, "Smooth subdivision of tetrahedral meshes," in *Eurographics/ACM SIGGRAPH Symposium on Geometry Processing*, 2004, pp. 147–154.
- [13] J. A. Brentzen, R. Abdashitov, and K. Singh, "Interactive shape modeling using a skeleton-mesh co-representation," *ACM Transactions on Graphics*, vol. 33, no. 4, pp. 1–10, 2014.
- [14] I. V. Guskov, P. Schroeder, and W. Sweldens, "Non-uniform relaxation procedure for multiresolution mesh processing," US patent, 2014.
- [15] Y. Zhang and L. Ma, "A scaling method of sensitive objects based on loss constraint triangle mesh deformation," *International Journal of Image and Graphics*, vol. 3, no. 2, pp. 77–83, 2015.
- [16] J. Tao, J. Carson, L. Liu, J. Warren, M. Bello, and I. Kakadiaris, "Subdivision meshes for organizing spatial biomedical data," *Methods*, vol. 50, no. 2, pp. 70–76, 2010.
- [17] D. Zorin, P. Schroder, and W. Sweldens, "Interpolating subdivision for meshes with arbitrary topology," in *ACM SIGGRAPH*, 1996, pp. 189–192.
- [18] C. T. Loop, "Smooth subdivision surfaces based on triangles," *Department of Mathematics the University of Utah Masters Thesis*, 1987.
- [19] E. Catmull and J. Clark, "Recursively generated B-spline surfaces on arbitrary topological meshes," *Computer-Aided Design*, vol. 10, no. 6, pp. 350–355, 1978.
- [20] Q. Xie, K. Y. Sze, and Y. X. Zhou, "Drape simulation using solid-shell elements and adaptive mesh subdivision," *Finite Elements in Analysis and Design*, vol. 106, pp. 85–102, 2015.
- [21] H. H. Liu, "An improved refinement algorithm of triangular mesh subdivision based on minimum weight theory," *Applied Mechanics and Materials*, vol. 513-517, pp. 2552–2555, 2014.
- [22] A. Amresh, G. Farin, and A. Razdan, "Adaptive subdivision schemes for triangular meshes," in *Hierarchical and Geometrical Methods in Scientific Visualization*, 2002, pp. 319–327.
- [23] D. Rose, M. Kada, and T. Ertl, "On-the-fly adaptive subdivision terrain," in *Vision Modeling and Visualization Conference*, 2001, pp. 87–92.
- [24] L. Kobbelt, " $\sqrt{3}$ -subdivision," *ACM Transactions on Graphics (SIGGRAPH)*, vol. 18, no. 1, pp. 103–112, 2000.
- [25] S. Seeger and H. Kai, "A sub-atomic subdivision approach," in *Vision Modeling and Visualization Conference*, 2001, pp. 77–86.
- [26] Q. Li, J. Ye, and C. Kambhamettu, "Interest point detection using imbalance oriented selection," *Pattern Recognition*, vol. 41, no. 2, pp. 672–688, 2008.